diffraction in $CC'D'D$ will take the path shown by the heavy line in Fig. 2.7.2.4, simplifying the picture to the case of extreme confinement of energy flow to parallelism with the Bragg planes. At the X-ray exit surface DD', splitting into $\mathbf{K}_0$ and $\mathbf{K}_h$ beams occurs. A slit-less arrangement, as shown in the figure, may suffice. Then, when S is a point-like source of $K\alpha$ radiation, and distance a is sufficiently large, films F_1 and F_2 will each record a pair of narrow images formed by the α_1 and α_2 wavelengths, respectively. A wider area of specimen can be imaged if a line focus rather than a point focus is placed at S (Barth & Hosemann, 1958), but then the α_1 and α_2 images will overlap. Under conditions of high anomalous transmission, defects in the crystal cause a reduction in transmitted intensity, which appears similarly in the $\mathbf{K}_0$ and $\mathbf{K}_h$ images. Thus, it is possible to gain intensity and improve resolution by recording both images superimposed on a film F_3 placed in close proximity to the X-ray exit face DD' (Gerold & Meier, 1959).

2.7.3. Double-crystal topography

The foregoing description of single-crystal techniques will have indicated that in order to gain greater sensitivity in orientation contrast there are required incident beams with closer collimation, and limitation of dispersion due to wavelength spread of the characteristic X-ray lines used. It suggests turning to prior reflection of the incident beam by a perfect crystal as a means of meeting these needs. Moreover, the application of crystal-reflection-collimated radiation to probe angularly step by step as well as spatially point by point the intensity of Bragg reflection from the vicinity of an individual lattice defect such as a dislocation brings possibilities of new measurements beyond the scope provided by simply recording the local value of the integrated reflection. The X-ray optical principles of double-crystal X-ray topography are basically those of the double-crystal spectrometer (Compton & Allison, 1935). The properties of successive Bragg reflection by two or more crystals can be effectively displayed by a Du Mond diagram (Du Mond 1937), and such will now be applied to show how collimation and monochromatization result from successive reflection by two crystals, U and V, arranged as sketched in Fig. 2.7.3.1. They are in the dispersive, antiparallel, '$++$' setting, and are assumed to be identical perfect crystals set for the same symmetrical Bragg reflection. Only rays making the same glancing angle with both surfaces will be reflected by both U and V. For example, radiation of shorter wavelength reflected at a smaller glancing angle at U (the ray shown by the dashed line) will impinge at a larger glancing angle on V and not satisfy the Bragg condition. In this $++$ setting, with a given angle ω between the Bragg-reflecting planes of each crystal, $\theta_U + \theta_V = \omega$ and $\Delta\theta_U = -\Delta\theta_V$. The Du Mond diagram for the $++$ setting, Fig. 2.7.3.2, shows plots of Bragg's law for each crystal, the V curve being a reflection of the U curve in a vertical mirror line and differing by ω from the U curve in its coordinate of intersection with the axis of abscissa, in accord with the equations given above. The small angular range of reflection of a monochromatic ray by each perfect crystal is represented exaggeratedly by the band between the parallel curves. Where the band for crystal U superimposes on the band for V (the shaded area) defines semiquantitatively the divergence and wavelength spread in the rays successively reflected by U and V. (It is taken for granted that $\frac{1}{2}\omega$ lies between the maximum and minimum incident glancing angles on U, $\theta_{\max}$ and $\theta_{\min}$, afforded by the incident beam, assumed polychromatic.) The reflected beam from U alone contains wavelengths ranging from $\lambda_{\min}$ to $\lambda_{\max}$. Comparison of these θ and λ ranges with the extent of the shaded area illustrates the efficacy of the $++$ arrangement in providing a collimated and monochromatic beam, which can be employed to probe the reflecting properties of a third crystal (Nakayama, Hashizume, Miyoshi, Kikuta & Kohra, 1973). Techniques employing three or more successive Bragg reflections find considerable application when used with synchrotron X-ray sources, and will be considered below, in Section 2.7.4.

The most commonly used arrangement for double-crystal topography is shown in Fig. 2.7.3.3, in which U is the 'reference' crystal, assumed perfect, and V is the specimen crystal under examination. Crystals U and V are in the parallel, '$+-$' setting, which is non-dispersive when the Bragg planes of U and V have the same (or closely similar) spacings. Before considering the Du Mond diagram for this arrangement, note that Bragg reflection at the reference crystal U is asymmetric, from planes inclined at angle α to its surface. Asymmetric reflections have useful properties, discussed, for example, by Renninger (1961), Kohra (1972), Kuriyama & Boettinger (1976), and Boettinger, Burdette & Kuriyama (1979). The asymmetry factor, b, of magnitude $|\mathbf{K}_0 \cdot \mathbf{n}/\mathbf{K}_h \cdot \mathbf{n}|$, $\mathbf{n}$ being the

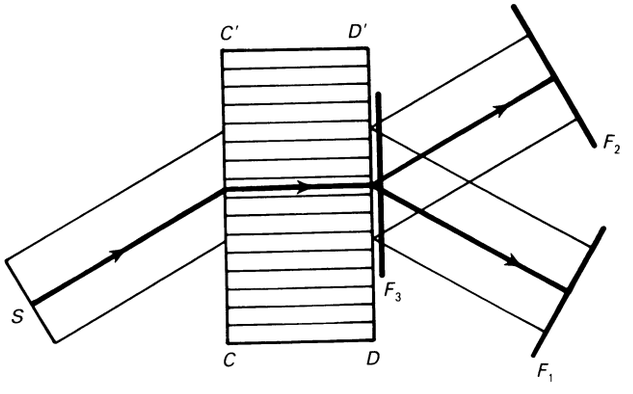

Fig. 2.7.2.4. Topographic techniques using anomalous transmission.

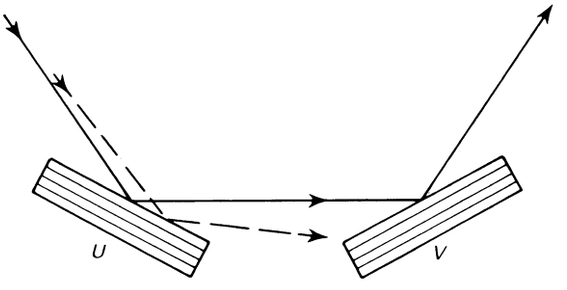

Fig. 2.7.3.1. Double-crystal $++$ setting.

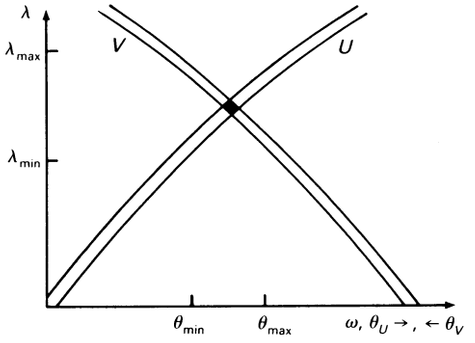

Fig. 2.7.3.2. Du Mond diagram for $++$ setting in Fig. 2.7.3.1.

crystal-surface normal, is also the ratio of spatial widths of the incoming to the outgoing beams, W_{in}/W_{out}. In the case of symmetric Bragg reflection, the perfect crystal U would totally reflect (in the zero-absorption case) over a small angular range, w_S. In the asymmetric case, the ranges of total reflection are w_{in} for the incoming rays and w_{out} for the outgoing. Dynamical-diffraction theory [*IT* B (1996, Part 5)] shows that $w_{out} = bw_{in} = b^{1/2} w_S$, so that $w_{in}W_{in} = w_{out}W_{out}$ (as would be expected from energy conservation). Thus, highly asymmetric reflection from the reference crystal U not only provides a spatially wide beam, able to cover a large area of V without recourse to any mechanical traversing motion of the components S, U or V, but also produces a desirably narrow angular probe for studying the angular breadth of reflection of V. In practice, values of b lower than 0.1 can be used.

Du Mond diagrams for the $+-$ arrangement are shown in Fig. 2.7.3.4(*a*) and (*b*). For simplicity, the curves (slope $d\lambda/d\theta = 2d\cos\theta$) are represented by straight lines. In the $+-$ setting, $\theta_V - \theta_U = \omega$ and $\Delta\theta_V = \Delta\theta_U$. In Fig. 2.7.3.4(*a*), the narrow band labelled U passing through the origin represents the beam of angular width w_{out} leaving U. It is assumed that all of the specimen crystal V has the same interplanar spacing as U but that it contains a slightly misoriented minor region V'(which may be located as shown in Fig. 2.7.3.3). When ω differs substantially from zero, the bands corresponding to crystal V and its minor part V' lie in positions V_1 and V_1', respectively, in Fig. 2.7.3.4(*a*). (Only the relevant part of the latter band is drawn, for simplicity.) The offset along the θ axis between V_1 and V_1' is the component $\Delta\varphi$ of the misorientation between V and V' that lies in the plane of incidence. If ω is reduced step-wise, a double-crystal topograph image being obtained at F at each angular setting, $\Delta\varphi$ can be found from film densitometry, which will show at what settings band U is most effectively overlapped by band V or by band V'. When ω is reduced to zero, the specimen crystal bands are at V_2 and V_2'. The drawing shows that V' has then passed right through the setting for its Bragg reflection, which occurred at a small positive value of ω. Since the U and V bands have identical slopes, their overlap occurs at all wavelengths when $\omega = 0$. In practice, only the shaded area is involved, corresponding to the wavelength range λ_{min} to λ_{max}, defined by the range of incidence angles, θ_{min} to θ_{max}, on the Bragg planes of crystal U. (The width of band U will generally be negligible compared with the range of θ allowed by source width and slit collimation system.) One component of $\Delta\varphi$ is found in the procedure just described. The second component needed to specify the difference between **h**-vector directions of the Bragg planes of V and V' is obtained by repeating the experiment after rotating V by 90° about **h**.

Next consider the more general case when V' differs from V in both orientation and interplanar spacing, and both V' and V have slightly different interplanar spacings from U. The difference in orientation between V' and V, $\Delta\varphi$, and their difference in interplanar spacing, $d(V') - d(V)$, can be distinguished by taking two series of double-crystal topographs, the orientation of the specimen in its own plane (its azimuthal angle, ψ) being changed by a 180° rotation about its **h** vector between taking the first and second series. As shown schematically in the Du Mond diagram, Fig. 2.7.3.4(*b*), the U, V, and V' bands now all have slightly different slopes. [Reference crystal U is reflecting the same small wavelength band as in Fig. 2.7.3.4(*a*).] The setting represented in the diagram is that putting V at the maximum of its Bragg reflection Let the V' band be then at position V_0', for the case when $\psi = 0°$. Assume that, when ψ is changed by 180°, the rotation of the specimen in its own plane can be made about the **h** vector of V precisely. (This assumption simplifies the diagram.) Then this 180° rotation will not cause any translation of the V band along the θ axis, but does transfer the V' band from V_0' to the position V_{180}'. With the sense of increasing ω taken as that translating the specimen bands to the right and $\Delta\omega$ taken as the difference in readings between peak reflection from V and that from V', the diagram shows that, with $\psi = 0°$, $\Delta\omega_0 = \theta(V') - \theta(V) + \Delta\varphi$, and, with $\psi = 180°$,

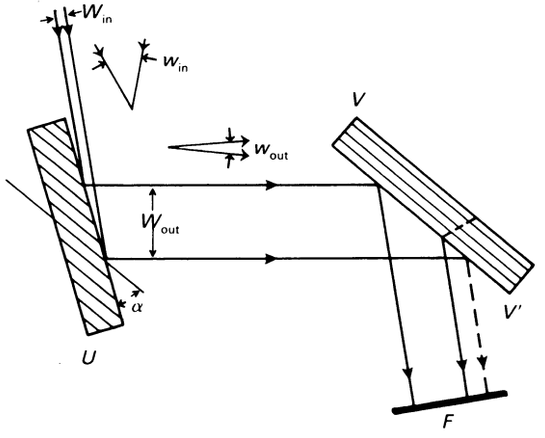

Fig. 2.7.3.3. Double-crystal topographic arrangement, $+-$ setting. Asymmetric reflection from reference crystal U. Specimen crystal divided into regions V and V'.

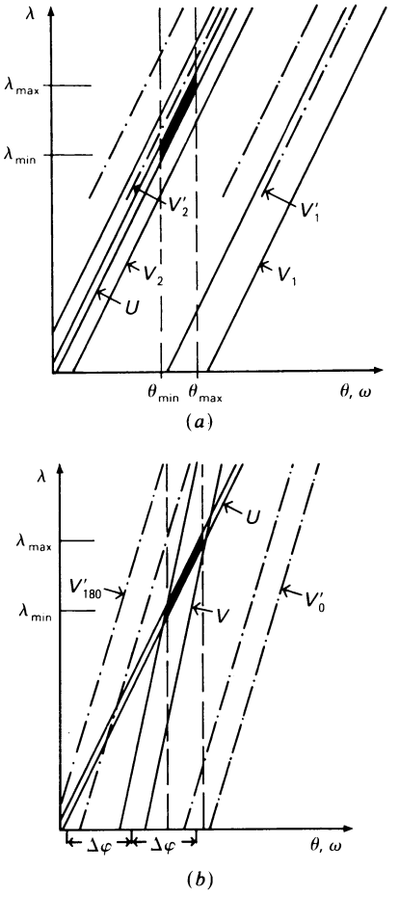

Fig. 2.7.3.4. Du Mond diagrams for $+-$ setting in Fig. 2.7.3.3. (*a*) Case when specimen region V' is misoriented with respect to V, but U, V, and V' all have the same interplanar spacing. (*b*) Case when V' differs from V in both orientation and interplanar spacing, and both differ from U in interplanar spacing.

$\Delta\omega_{180} = \theta(V') - \theta(V) - \Delta\varphi$, from which both $\Delta\varphi$ and the difference in Bragg angles can be found. The interplanar spacing difference is given by $d(V') - d(V) = [\theta(V) - \theta(V')]\bar{d}\cot\theta$, $\bar{d}$ being the mean interplanar spacing of V and V'. In practice, series of topographs are taken with azimuthal angles $\psi = 0$, 90, 180, and 270°, so that the two components needed to specify the misorientation vector between the Bragg-plane normals of V and V' can be determined. The Du Mond diagram shows that in this slightly dispersive experiment the range of overlap of the U band with any V band can be restricted by reducing the angular range or wavelength range of rays incident on U. Such reduction can be achieved by use of a small source S far distant from U, such as a synchrotron source. It can also be achieved by methods described in Subsection 2.7.4.2. As regards spatial resolution on double-crystal topographs, relations analogous to those for single-crystal topographs apply. If the reference crystal U unavoidably contains some defects, their images on F can deliberately be made diffuse compared with images of defects in V by making the UV distance relatively large. In a nearly dispersion-free arrangement, if the $K\alpha_1$ wavelength is being reflected, then so too will the $K\alpha_2$ if S is sufficiently widely extended in the incidence plane, as is usually necessary to image a usefully large area of V. If the distance VF cannot be made sufficiently small to reduce to a tolerable value the resolution loss due to simultaneous registration of the α_1 and α_2 images, then a source S of small apparent size, together with a collimating slit before U, will be needed. In order to obtain imaging of a large area of V, a linear scanning motion to and fro at an angle to SU in the plane of incidence must be performed by the source and collimator relative to the double-crystal camera. Whether it is the source and collimator or the camera that physically move depends upon their relative portability. When the source is a standard sealed-off X-ray tube, it is not difficult to arrange for it to execute the motion (Milne, 1971).

In some applications, it may occur that the specimen is so deformed that only a narrow strip of its surface will reflect at each ω setting. Then, a sequence of images can be superimposed on a single film, changing ω by a small step between each exposure. The 'zebra' patterns so obtained define contours of equal 'effective misorientation', the latter term describing the combined effect of variations in tilt $\Delta\varphi$ and of Bragg-angle changes due to variations in interplanar spacing (Renninger, 1965; Jacobs & Hart, 1977).

Double-crystal topography employing the parallel setting was developed independently by Bond & Andrus (1952) and by Bonse & Kappler (1958), and used by the former workers for studying reflections from surfaces of natural quartz crystals, and by the latter for detecting the strain fields surrounding outcrops of single dislocations at the surfaces of germanium crystals. Since then, the method has been much refined and widely applied. The detection of relative changes in interplanar spacing with a sensitivity of 10^{-8} is achievable using high-angle reflections and very perfect crystals. These developments have been reviewed by Hart (1968, 1981).

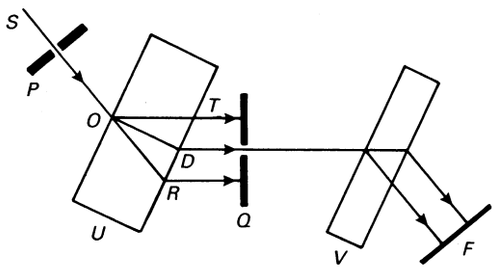

Fig. 2.7.3.5. Transmission double-crystal topography in + − setting with spatial limitation of beam leaving reference crystal.

Transmitted Bragg reflection (*i.e.* the Laue case) can be used for either or both crystals U and V, in both the + + and + − settings, if desired. When the reference crystal U is used in transmission, a technique due to Chikawa & Austerman (1968), shown in Fig. 2.7.3.5, can be employed if U is relatively thick and, preferably, not highly absorbing of the radiation used. This technique exploits a property of diffraction by ideally perfect crystals, that, for waves satisfying the Bragg condition exactly, the energy-flow vector (Poynting vector) within the energy-flow triangle (the triangle *ORT* in Figs. 2.7.2.2 and 2.7.2.3) is parallel to the Bragg planes. (In fact, the energy-flow vectors swing through the triangle *ORT* as the range of Bragg reflection is swept by the incident wave vector, $\mathbf{K}_0$.) Placing a slit Q as shown in Fig. 2.7.3.5 so as to transmit only those diffracted rays emerging from *RT* whose energy-flow direction in the crystal ran parallel, or nearly parallel, to the Bragg plane *OD* has the effect of selecting out from all diffracted rays only those that have zero or very small angular deviation from the exact Bragg condition. The slit Q thus provides an angularly narrower beam for studying the specimen crystal V than would be obtained if all diffracted rays from U were allowed to fall on V. The specimen is shown here in the + − setting, and also oriented to transmit its diffracted beam to the film F. This specimen arrangement is a likely embodiment of the technique but is incidental to the principle of employing *spatial* selection of transmitted diffraction rays to gain *angular* selection, a technique first used by Authier (1961). A practical limitation of this technique arises from angular spreading due to Fraunhofer diffraction by the slit Q: use of too fine an opening of Q will defeat the aim of securing an extremely angularly narrow beam for probing the specimen crystal.

2.7.4. Developments with synchrotron radiation

2.7.4.1. *White-radiation topography*

The generation and properties of synchrotron X-rays are discussed by Arndt in Subsection 4.2.1.5. For reference, his list of important attributes of synchrotron radiation is here repeated as follows: (1) high intensity, (2) continuous spectrum, (3) narrow angular collimation, (4) small source size, (5) polarization, (6) regularly pulsed time structure, and (7) computability of properties. All these items influence the design and scope of X-ray topographic experiments with synchrotron radiation, in some cases profoundly. The high intensity of continuous radiation delivered in comparison with the output of standard X-ray tubes, and hence the rapidity with which X-ray topographs could be produced, was the first attribute to attract attention, through the pioneer experiments of Tuomi, Naukkarinen & Rabe (1974), and of Hart (1975*a*). They used the simple diffraction geometry of the Ramachandran (Fig. 2.7.1.2) and Schulz (Fig.2.7.1.1) methods, respectively. [Since in the transmission-specimen case a multiplicity of Laue images can be recorded, it is usual to regard this work as a revival of the Guinier & Tennevin (1949) technique.] Subsequent developments in synchrotron X-ray topography have been reviewed by Tanner (1977) and by Kuriyama, Boettinger & Cohen (1982), and described in several chapters in Tanner & Bowen (1980). Some developments of methods and apparatus that have been stimulated by the advent of synchrotron-radiation sources will be described in this and in the following Subsection 2.7.4.2, the division illustrating two recognizable streams of development, the first exploiting the speed and relative instrumental simplicity

references